Ion beam analysis of as-received, H-implanted and post implanted annealed fusion steels

R. Gonzalez-Arrabal , F. Munnik , M. González , P. Romero , R. Heller , F. Leardini , J.M. Perlado

A B S T R A C T

The elemental distribution for as-received (AR), H implanted (AI) and post-implanted annealed (A) Eurofer and ODS-Eurofer steels has been characterized by means of micro Particle Induced X-ray Emission (μ-PIXE), micro Elastic Recoil Detection (μ-ERD) and Secondary Ion Mass Spectrometry (SIMS). The temperature and time-induced H diffusion has been analyzed by Resonance Nuclear Reaction Analysis (RNRA), Thermal Desorption Spectroscopy (TDS), ERDA and SIMS techniques. μ-PIXE measurements point out the presence of inhomogeneities in the Y distribution for ODS-Eurofer samples. RNRA and SIMS experiments evidence that hydrogen easily outdiffuses in these steels even at room temperature. ERD data show that annealing at temperatures as low as 300 °C strongly accelerates the hydrogen diffusion process, driving out up to the 90% of the initial hydrogen.

1. Introduction

The development of high-performance structural materials that can withstand the harsh conditions (high thermal loads and flux of energetic neutrons) of a fusion reactor is one of the main challenges for materials scientifics. Selection criteria for this kind of materials are mainly based on their thermophysical, mechanical, radiation resistance, activation and corrosion properties. After a long and intense research, nowadays ferritic/martensitic steels such as Eurofer and oxide dispersion strengthened Eurofer (ODS-Eurofer) have been proposed as one of the best candidates to be located in fusion reactors [1–3]. The high fluxes of neutrons impinging on these kind of materials significantly deteriorate their properties mainly as a consequence of two different type of interaction between the radiation particles and the target atoms: (i) atomic displacement thus, Frenkel pair formation and (ii) creation of light species (H, D, He, ...) via transmutation reactions. Apart from the atomic displacement, the presence of foreign light species in steels and particularly their precipitation into bubbles notably deteriorates the mechanical properties of the material (enhancement of embrittlement and swelling) [4–6] limiting somehow their lifetime. It is important to remark that the predicted amount of light species generation is at least one order of magnitude higher in fusion than in fission reactors [7]. Because of these reasons, the study and understanding of the foreign species behavior (diffusion and/or retention) in the steel matrix is a key point in further material development for fusion applications. Previous works [8] demonstrate that refining the steel microstructure (e.g. introduction of nano-precipitates in steels) provides a sink for radiation-induced defects and light atoms, improving the radiation resistance and high temperature properties (creep strength and oxidation/corrosion resistance) of conventional steels. In the last years quite a lot of effort has been made to control and define the crystal structure, number density, size distribution and interfacial structure of oxide nanoparticles in ODS-steels in order to attain the required material properties [9]. Nevertheless, further research has to be carried out in order to achieve steels with the mandatory characteristics for DEMO.

The aim of this paper is to characterize the elemental distribution (in particular the Y distribution within the ODS-Eurofer matrix) and the H depth profiling in AR, AI and A Eurofer and ODS-Eurofer steels. Moreover, the feasibility of employing a nuclear microprobe (using MeV ions) to investigate the correlation between the Y and the H distribution in ODS-Eurofer steels is explored.

2. Experimental

A brief overview of the studied samples, treatments and experimental techniques used for their characterization is listed in Table 1.

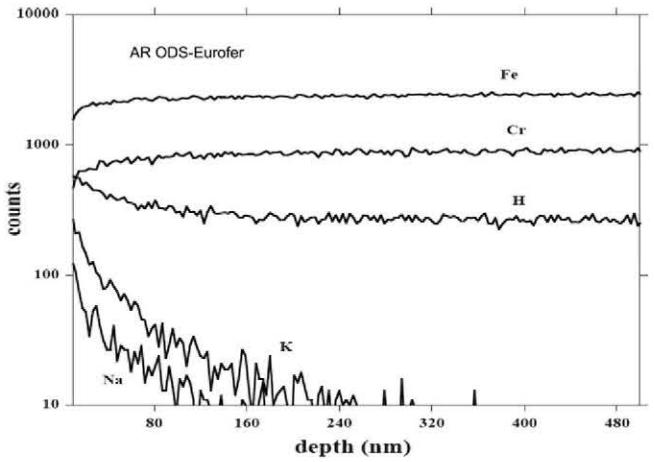

Fig. 1. Elemental depth profile for an AR ODS-Eurofer as measured by SIMS.

Eurofer and ODS-Eurofer steel samples were cut from as-received batches in pieces of $15 \times 40 \times 1$ mm^3. The samples surface was finished by lamination at suppliers. Some of the as-received steel samples were then implanted with H at an energy of 50 keV at a fluence of 3×10^{17} ions/cm^{-2} at room temperature. Because of the difficulty to measure hydrogen (it is a very small atom with a quite low cross section and strongly mobile), the selection of the implantation parameters (energy and dose) was done to favor the analysis. Thus, the energy was selected to have the hydrogen at a depth in which neither the multiple scattering nor the surface effects dominate, whereas the dose was selected in order to have a relatively good statistic in its detection. The projected range for the implanted ions was calculated by the SRIM Monte Carlo code [10] to be ~294 nm. The as-implanted hydrogen maximum concentration was estimated to be ~27 at.%. Some of the implanted samples were annealed in Ar atmosphere at temperatures of 300 and 500 °C for 24 and 100 h. Prior to the analysis implanted and annealed samples were stored under environmental conditions.

μ-PIXE and μ-ERD spectra were simultaneously measured in order to characterize the elemental distribution of the samples and the possible correlation between the Y and the H distribution for H-implanted ODS-steels. For these measurements a He^+ beam at an energy of 2.4 MeV was used. The beam current was selected to be low (~1.2 nA) in order to avoid H diffusion during the measurements by ion irradiation. The total accumulated charge per map was around 1 μC. The beam current was measured in a Faraday cup at the entrance of the setup, positioned with an offset to the beam axis. The beam was electrostatically deflected into the Faraday cup on a regular basis during the measurement. The total charge was based on the sum of the product of current and effective measurement times between current measurements. This method does not depend on the problems of secondary electron production related to charge measurement on the sample. The beam spot was $\sim 5 \times 20\ \mu m^2$ and the total scan areas were $\sim 260 \times 260\ \mu m^2$. The characteristic emitted X-rays were collected by a Li-doped Si detector located at 120° to the beam direction. The

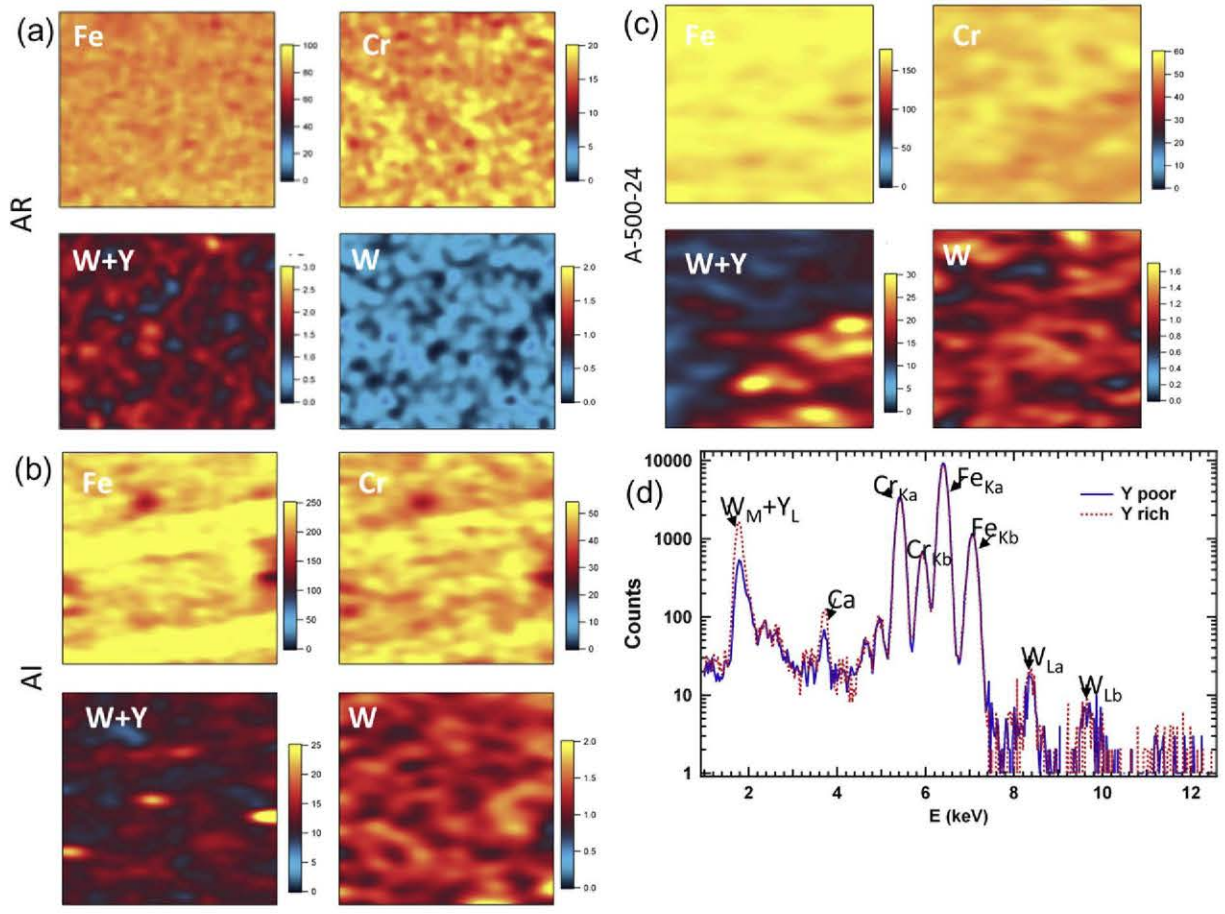

Fig. 2. Elemental distribution maps for (a) AR, (b) Al, (c) A-500-24 ODS-Eurofer samples. The dimensions of the maps are $260 \times 260\ \mu m^2$. (d) PIXE spectra taken at regions with different Y content of an Al ODS-Eurofer sample: Y poor (blue line) and Y-rich (red dot line). (For interpretation of the references to color in this figure legend, the reader is referred to the web version of this article.)

recoil hydrogen atoms were measured by a partially depleted PIPS detector at a scattering angle of 30°. A 10 μm Al foil was placed in front of the detector to stop scattered He ions. In order to achieve the optimal experimental configuration which allows simultaneously measuring PIXE and ERD spectra, the samples were tilted 15° to the beam direction (angle between beam direction and sample normal 75°). The home-build CAMAC based acquisition system KMS was used for the measurements. Further details of the microbeam line can be found in Ref. [11].

For comparison, compositional analyses were also performed on a ToFSIMS type ION-TOF IV instrument. Sputter etching of the surface was accomplished with a beam of 2 keV Cs^+ ions raster over a $300 \times 300\ \mu m^2$ area. A pulsed beam of 25 keV Bi^+ ions, scanned over a $50 \times 50\ \mu m^2$ region centred within the sputtered area, was used to generate secondary ions for analysis in negative ion mode. A high current beam of low energy (<20 eV) electrons was employed for charge compensation. Mass resolution was higher than 6000. Depth values were provided by measuring the sputter crater using a Wyko NT1100 interferometer.

RNRA experiments were carried out by using the $H(^{15}N,He\gamma)^{12}C$ [12] nuclear reaction with a N^{2+} beam impinging onto the sample surface at normal incidence. This reaction has a sharp resonance at 6.385 MeV. The beam energy was varied in the range from 6.485 to 7.385 MeV. The 4.43 MeV γ-rays were detected by a 4 × 4 inch BGO detector mounted immediately outside the vacuum about 1.5 cm behind the sample. Some special precautions were taken into account in order to carry out reliable depth profiling measurements and to avoid ion beam-induced hydrogen diffusion [13,14]. The beam spot and the current were selected to be $3 \times 3\ mm^2$ and ~10 nA, respectively. Besides, the beam spot position was changed every two measurements. Several spectra were sequentially measured on the same point up to a dose 10 times higher than the used in real experiments and no ion beam-induced hydrogen diffusion was detected.

The hydrogen release as a function of temperature was characterized by means of Thermal Desorption Spectroscopy (TDS). TDS has been accomplished in a Differential Scanning Calorimeter (Perkin–Elmer mod. DSC-4) coupled to a Quadrupole Mass Spectrometer (Balzers, mod. Prisma). Further details of the experimental system and the calibration experiments performed to quantify the hydrogen desorbed flow can be found elsewhere [15].

3. Results and discussion

3.1. Elemental distribution characterization

The elemental distribution was characterised by μ-PIXE and SIMS techniques. Typical SIMS spectra for an AR ODS-Eurofer sample are shown in Fig. 1. μ-PIXE (see Fig. 2d) and SIMS data illustrate that samples are composed by main matrix elements (Cr, Fe and W) and Y for the ODS-Eurofer steel. It is also important to mention the presence of K and Ca on the sample surface which can be considered as contaminants. Moreover, H is detected along the whole sample thickness. Since the samples were fabricated in a H_2 atmosphere these results indicate that some H might incorporate into the steel matrix during the manufacturing process.

As depicted in Table 1, μ-PIXE elemental distribution maps were measured for all studied samples. Maps were estimated from the defined region of interests (ROIs) corresponding to the W_L, $Fe_{K\alpha+K\beta}$ and $Cr_{K\alpha}$ peaks for Eurofer plus W_M, $+Y_L$ peak for the ODS-Eurofer. Because of the experimental conditions the W_M and Y_L peaks overlap. However, the presence of Y in the samples can be deduced from the increase in the peak high and width (see Fig. 2d). Because of this reason an accurate quantification of the Y content is not possible. Nevertheless, this topic falls out of the scope of this paper. For clarity, Fig. 2 shows maps corresponding to representative samples (AR, AI, and A500-24 ODS-Eurofer). μ-PIXE measurements evidence that all studied elements are homogeneously distributed within the whole characterised area for the AR, AI and post-implanted annealed Eurofer (not shown). The elemental distribution is also observed to be quite homogeneous for three of the six studied ODS-Eurofer samples: AR, A300-24 (not shown) and A300-100 (not shown). In the other three ODS-Eurofer samples (AI, A500-24, and A500-100), a high color contrast is observed in some small regions of the maps corresponding to W_M plus Y_L (see Figs. 2b and c and 3). Since, as illustrate in the maps and in Fig. 2d, in these samples the $W(W_L)$ distribution is

Table 1
Brief overview of sample codes, treatments and experimental techniques used for the analysis.

Material	Sample code	H-implanted	Annealing temperature (°C)	Annealing time (h)	μ-ERDA	μ-PIXE	RNRA	TDS	SIMS
Eurofer	AR					X			X
Eurofer	AI	X			X	X	X		X
ODS-Eurofer	AR					X		X	X
ODS-Eurofer	AI	X			X	X	X	X	X
ODS-Eurofer	A300-24	X	300	24	X	X			
ODS-Eurofer	A300-100	X	300	100	X	X			
ODS-Eurofer	A500-24	X	500	24	X	X			
ODS-Eurofer	A500-100	X	500	100	X	X			

*The sample code (AX00-00) corresponds to: A, annealed sample; X00, annealing temperature; and 00, annealing time.

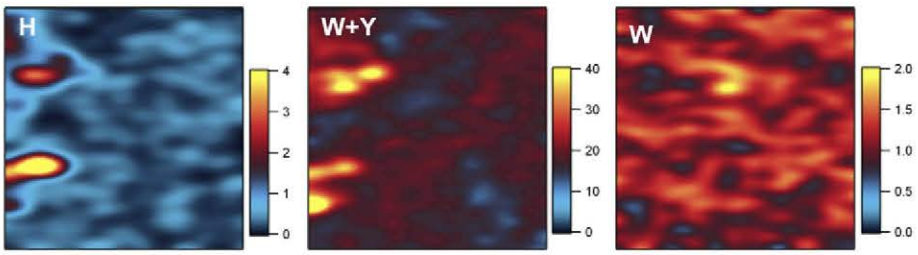

Fig. 3. Elemental distribution maps for H-implanted and annealed at 500 °C for 100 h ODS-Eurofer steel. The dimensions of the maps are $260 \times 260\ \mu m^2$.

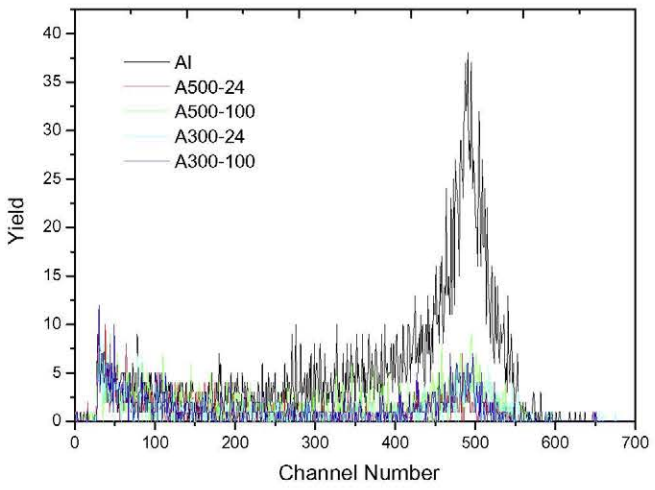

Fig. 4. ERDA spectra for ODS-Eurofer samples after H implantation and after different annealing treatments.

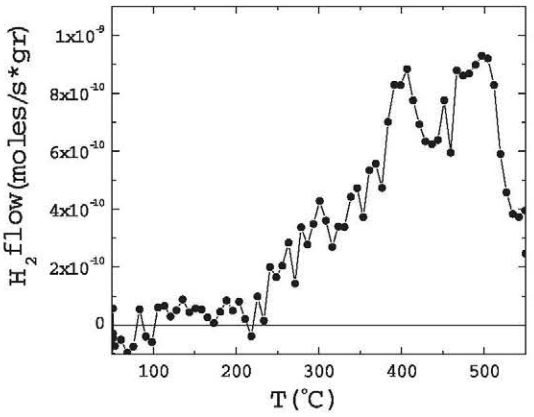

Fig. 5. Thermal desorption spectra of an Al ODS-Eurofer sample. The H_2 desorbed flow per mass unit of sample has been calculated from the mass spectrometric ionic current i_2 by using an experimentally determined calibration factor. The spectrum has been obtained between 50 and 550 °C by applying a constant heating rate of 40 °C/min.

quite homogeneous; this contrast might correspond to regions in which Y might be more abundant. Thus, the existence of randomly distributed Y-rich regions with a size ranging from 5×40 to $20 \times 40\ \mu m^2$, can be deduced. The Y-rich zones correspond with Fe- and Cr-depleted zones indicating that, as expected, Y might be present in the matrix in the form of secondary phases which might substitute Fe and/or Cr as main matrix elements.

Since all the tested steels are supplied thermally treated (up to 700 °C) to obtain a fully martensitic microstructure that should remain stable during service, and considering that an inhomogeneous Y distribution is appreciated in annealed as well as, in non annealed samples, one can conclude that the origin of the inhomogeneities in Y distribution are related to the fabrication conditions and not to the additional treatments (implantation and/or annealing). Alves et al. [16] have previously reported an uneven Y distribution (20–50 μm Y depleted zones) for some similar as-received samples. Furthermore, it is important to remark that this result is not incoherent with that previously reported from TEM images in which usually a homogeneous distribution of Y particles with nanometer size is observed [17,18]. By comparing TEM and IBA results and considering the different length and depth scales of both methods, one can conclude that Y distribution which seems to be homogeneous in a nanometer scale turns out to be inhomogeneous when increasing the observation scale. It is important to take this result into consideration when studying the mechanical properties of this kind of materials.

3.2. Study of the relation between the Y and H distribution in H-implanted ODS steels

The role of the Y particle surfaces on H trapping is still a matter of controversy. Some previous works reported about its positive role in H trapping [19,20] while others conclude the opposite [21]. Therefore, in order to clarify this point μ-PIXE and μ-ERDA maps were simultaneously measured for those samples in which an inhomogeneous distribution of Y was observed (Al, A500-24 and A500-100). A correlation between the Y and the H distribution is only observed for the A500-100 sample. The maps corresponding to W_M plus Y_L, to W_L and to H for this sample are shown in Fig. 3. These data seems to indicate the possibility of investigating the correlation between the Y and the H distribution in the ODS-Eurofer steel by using a nuclear microprobe. Nevertheless, further studies are in progress to understand the reason for having correlation in this sample and not in the others and to find out if hydrogen was mainly located in the Y-rich regions right after the implantation or if on the contrary, it has migrated and got pinned there because of the thermal annealing.

3.3. Temperature and time-induced H diffusion

ERD measurements were carried out in order to study the annealing induced hydrogen diffusion. These measurements were done in a first set of samples 60 days after implantation. ERD

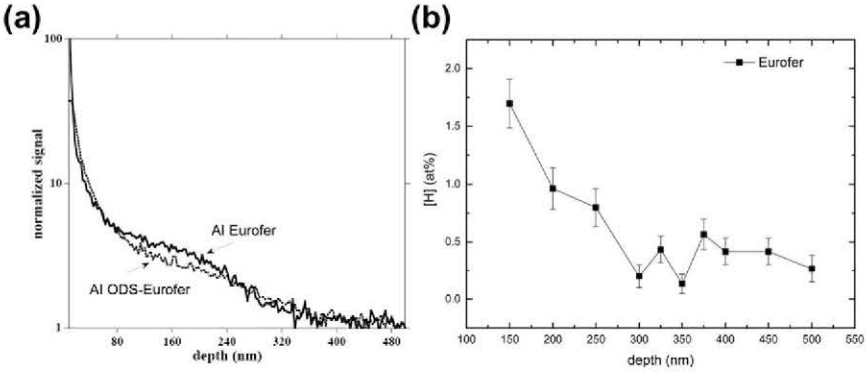

Fig. 6. (a) H depth profiling for Al Eurofer (black solid line) and Al ODS-Eurofer (black dots) steels as measured by SIMS 100 days after implantation, (b) H concentration as a function of depth for an Al Eurofer sample as measured by RNRA 120 days after implantation.

spectra taken for Al and post-implanted annealed ODS-Eurofer samples are shown in Fig. 4. In contrast to SRIM data in which H is calculated to be implanted at a depth of ~294 nm, ERD data illustrate that H is only present in a region close to the sample surface. As shown bellow, this result is further corroborated by SIMS and RNRA measurements. A significant decrease in the total yield, up to ~90%, is observed for all post-implanted annealed samples indicating that the thermal treatments at these temperatures drive the hydrogen to outdiffuse. These results agree quite well with those obtained from TDS experiments carried out in an Al sample which evidence that H starts to release from the sample at temperatures as low as 250 °C (Fig. 5).

In order to obtain better resolution, the hydrogen depth profile of a second set of samples was characterized 100 and 120 days after implantation by SIMS and RNRA, respectively. As depicted in Fig. 6a, and in Fig. 6b the H concentration increases with decreasing depth having a maximum near the sample surface. These data indicate that H releases from the steels when they are stored at ambient conditions.

In order to investigate the loss of H, its concentration is measured by RNRA at the same depth (~294 nm) as a function of time elapsed after implantation (Fig. 7). These data show that the H concentration in the samples has decreased by a factor of ~10 (from ~6 to ~0.5 at.%) 60 days after the first measurement. Since both set of samples were cut from the same batch and simultaneously implanted, the only factor which might explain this apparent discrepancy is the time elapsed between measurements. Thus, these results show that H might diffuse with time even at room temperature.

The migration of hydrogen is quite complicated to describe, especially in polycrystalline samples in which the presence of defects and grain boundaries play an important role. Nevertheless, different models have been proposed to describe the movement of H towards the sample surface [22–24]. Besides, the sample surface can also play a major role in the dynamics of hydrogen release. Since the kinetics of hydrogen atoms might decrease at surface, the H atoms could have enough time to recombine with other H atoms forming molecules before being released. Moreover, the presence of a thin oxide layer at surface could produce a H trapping effect near the metal-oxide interface, which could be caused by the strain fields generated at that interface [25]. In addition, the presence of O impurities would produce the trapping of H atoms due to the creation of O—H bondings [26]. In our particular case, the influence of the steel surface on hydrogen release is deduced from RNRA and SIMS data. The enhancement of the hydrogen concentration close to the sample surface suggests that at least part of the hydrogen gets somehow trapped in the near surface regions. Additionally, as shown in Fig. 6a the hydrogen concentration close to the sample surface is higher for the ODS-Eurofer than for the Eurofer, which may be due to differences in the microstructure.

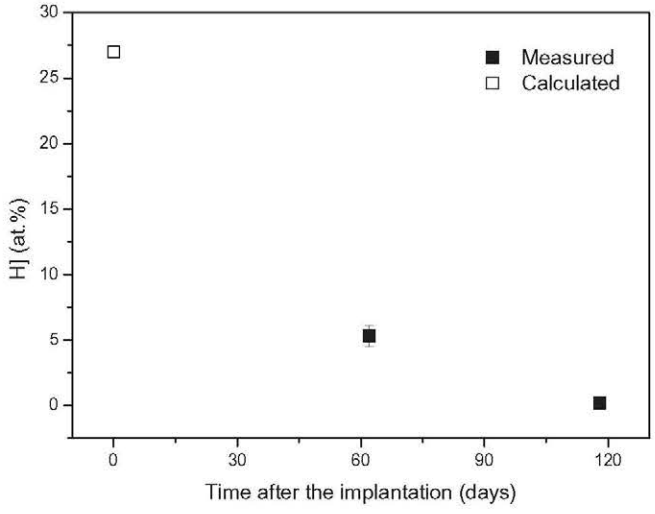

Fig. 7. H concentration as a function of time elapsed after the implantation as measured by RNRA (black squares) as calculated (opened squares). The H concentration has been measured at a depth of ~294 nm.

4. Conclusions

The elemental distribution of Eurofer and ODS-Eurofer steels has been characterized. Na and K impurities were found on the surface of both steels. Moreover, a small percentage of hydrogen was found along the whole investigated depth for as-received samples, which indicates that H incorporates into the steel during its manufacturing in a H_2-rich atmosphere. For ODS-Eurofer an inhomogeneous distribution of Y has been found for some of the samples, which might notably influence their mechanical properties.

By simultaneously measuring μ-PIXE and μ-ERDA maps, a correlation between Y and H distributions has been observed for a sample. These are preliminary data and in order to obtain more conclusive results further research has to be carried out.

Hydrogen is easily released from all studied steels; it even diffuses at room temperature. This room temperature diffusion is responsible for the strong decrease of the hydrogen concentration with time. The H depth profiles suggest that the sample surface might play an important role in the hydrogen outdiffusion. Indeed, a higher hydrogen concentration is detected in the near surface layers, which may indicate that the surface strongly reduces somehow the hydrogen releasing.

Heating the samples at temperatures as low as 300 °C (below operation temperature) strongly accelerates the hydrogen depletion process, driving the 90% of hydrogen to outdiffuse. The amount of released hydrogen has been found not to depend on the annealing conditions (time and temperature) for the selected range.

These results, even when very preliminary, show that hydrogen easily outdiffuse from future fusion steels which is very desirable to prevent swelling effects. Nevertheless, further research has to be done in order to mimic the hydrogen behavior under real reactor operation conditions.

Acknowledgments

IBA measurements were supported by the EU- "Research Infrastructures Transnational Access" program AIM "Center for Application of Ion Beams in Materials Research" under EC Contract No. 025646. The authors want to thank to Dr. P. Fernandez for providing the steels samples.

J.L. Boutard, A. Alamo, R. Landau, M. Rieth, C. R. Physique 9 (2008) 287.
S. Ukai, M. Fujiwara, J. Nucl. Mater. 307–311 (2002) 749.
A.A.F. Tavassoli et al., J. Nucl. Mater. 329–333 (2004) 257.
J.S. Lee, A. Kimura, S. Ukai, M. Fujiwara, J. Nucl. Mater. 329–333 (2004) 1122.
H. Trinkaus, B.N. Singh, J. Nucl. Mater. 323 (2003) 229.
K. Yutani, H. Kishimoto, R. Kasada, A. Kimura, J. Nucl. Mater. 367–370 (2007) 423.
IFMIF Comprehensive Design Report (IEA, Jan. 2004).
S. Ukai, M. Fujiwara, J. Nucl. Mater. 307–311 (2002) 749.
L.L. Hsiung, M.J. Fluss, S.J. Tumey, B.W. Choi, Y. Serruys, F. Willaime, A. Kimura, Phys. Rev. B 82 (2010) 184103.
J.F. Ziegler, M.D. Ziegler, and J.P. Biersack, SRIM-2006.02.
F. Herrmann, D. Grambole, Nucl. Instrum. Methods B 104 (1995) 26.
J.R. Tesmer, M. Nastasi, Handbook of Modern Ion Beam Materials Analysis, Pittsburgh, PA, MRS, 1995.

I.P. Chernov, A.P. Mamontov, Y.I. Tjurin, Y.P. Cherdantsev, J. Nucl. Mater. 233–237 (1996) 1118.
I.P. Chernov, A.P. Mamontov, Y.I. Tjurin, Y.P. Cherdantsev, M. Kröning, H. Baumbach, Int. J. Hydrogen Energy 24 (1999) 359.
J.R. Ares, F. Leardini, P. Díaz-Chao, J. Bodega, D.W. Koon, I.J. Ferrer, J.F. Fernández, C. Sánchez, J. Alloy. Compd. 495 (2010) 650.
L.C. Alves, E. Alve, A. Paúl, M.R. da Silva, J.A. Odriozol, Nucl. Instrum. Methods B 249 (2006) 493.
Y. Zhong Shen, H. Dong Cho, J. Jang, Nucl. Eng. Technol. 40 (2007) 99.
C. Eiselt, M. Klimenkov, R. Lindau, A. Möslang, H.R.Z. Sandim, A.F. Padilha, D. Raabe, J. Nucl. Mater. 385 (2009) 231.
J.S. Lee, A. Kimura, S. Ukai, M. Fujiwara, J. Nucl. Mater. 329–333 (2004) 1122.
G.A. Esteban, A. Peña, F. Legarda, R. Lindau, Fusion Eng. Des. 82 (2007) 2634.
V.V.V. Sagaradze, V.I. Shalaev, V.L. Arbuzov, B.N. Goshchitskii, Y. Tian, W. Qun, S. Jiguang, J. Nucl. Mater. 295 (2001) 265.
G.M. Pressouyre, Metall. Trans. A 10A (1979) 1571.
D.L. Johnson, G. Krauss, J.K. Wu, K.P. Tang, Metall. Trans. A 18A (1987) 717.
R.A. Oriani, Acta Metall. 18 (1970) 147.
L. Völk, G. Alefeld, Diffusion of Hydrogen in 'Metals in Hydrogen in Metals I', in: G. Alefeld, L. Völk (Eds.), Topics in Applied Physics, vol. 28, Springer, Berlin, 1978.
A. Wert, Trapping of Hydrogen in Metals in 'Hydrogen in Metals II', in: G. Alefeld, L. Völk (Eds.), Topics in Applied Physics, vol. 29, Springer, Berlin, 1978.